The Journal of Infectious Diseases

MAJOR ARTICLE

Homeostatic Expansion of CD4+ T Cells Promotes Cortical and Trabecular Bone Loss, Whereas CD8+ T Cells Induce Trabecular Bone Loss Only

M. Neale Weitzmann,[1,2,a] Tatyana Vikulina,[1,2] Susanne Roser-Page,[1] Masayoshi Yamaguchi,[2,b] and Ighovwerha Ofotokun[3,4,a]

[1]Atlanta Department of Veterans Affairs Medical Center, Decatur, and [2]Division of Endocrinology and Metabolism and Lipids and [3]The Division of Infectious Diseases, Department of Medicine, Emory University School of Medicine, and [4]Grady Healthcare System, Atlanta, Georgia

Background. Bone loss occurs in human immunodeficiency virus (HIV) infection but paradoxically is intensified by HIV-associated antiretroviral therapy (ART), resulting in an increased fracture incidence that is largely independent of ART regimen. Inflammation in the bone microenvironment associated with T-cell repopulation following ART initiation may explain ART-induced bone loss. Indeed, we have reported that reconstitution of CD3+ T cells in immunodeficient mice mimics ART-induced bone loss observed in humans. In this study, we quantified the relative effects of CD4+ and CD8+ T-cell subsets on bone.

Methods. T-cell subsets in T-cell receptor β knockout mice were reconstituted by adoptive transfer with CD4+ or CD8+ T-cells subsets were reconstituted in T-cell receptor β knockout mice by adoptive transfer, and bone turnover, bone mineral density, and indices of bone structure and turnover were quantified.

Results. Repopulating CD4+ but not CD8+ T cells significantly diminished bone mineral density. However, micro–computed tomography revealed robust deterioration of trabecular bone volume by both subsets, while CD4+ T cells additionally induced cortical bone loss.

Conclusions. CD4+ T-cell reconstitution, a key function of ART, causes significant cortical and trabecular bone loss. CD8+ T cells may further contribute to trabecular bone loss in some patients with advanced AIDS, in whom CD8+ T cells may also be depleted. Our data suggest that bone densitometry used for assessment of the condition of bone in humans may significantly underestimate trabecular bone damage sustained by ART.

Keywords. AIDS; antiretroviral therapy; ART; inflammation; osteoclasts; osteoporosis; T cells; HIV; bone loss.

Osteoclasts are bone-resorbing (ie, degrading) cells, and they differentiate from precursors that circulate among the monocyte lineage under the action of the key osteoclastogenic cytokine receptor activator of nuclear factor κB ligand (RANKL) in the presence of permissive concentrations of macrophage colony-stimulating factor (M-CSF). Osteoprotegerin, a decoy receptor for RANKL, moderates RANKL-induced osteoclastogenesis and bone resorption [1, 2]. A centralization of immune and skeletal functions around common cell types and shared cytokine effectors that serve discrete functions in both organ systems (ie, the immunoskeletal interface) has pronounced consequences for the skeleton both in the context of immune deficiency and in immune activation (ie, inflammatory) states. Human immunodeficiency virus (HIV) infection, a condition associated with both immunodeficiency and inflammation, is recognized to cause severe skeletal deterioration [3–8], and it is estimated that up to two thirds of HIV-infected patients have low bone mineral density (BMD; ie, osteopenia) and that up to 10% have osteoporosis [9–11].

The underlying pathology that gives rise to bone loss is poorly understood and likely multifactorial [5, 8], but we have investigated an immunocentric basis and reported that the human immunodeficiency virus type 1 (HIV) transgenic rat, an animal model of HIV infection, undergoes significant bone loss due to an elevated ratio of RANKL to osteoprotegerin expression in B cells [12]. Importantly, our recently translational clinical studies have revealed that an imbalance in the B-cell levels of RANKL to osteoprotegerin is a feature of human HIV infection and correlates significantly with diminished BMD in the appendicular skeleton [13].

Antiretroviral therapy (ART) is extremely effective in suppressing HIV replication, leading to rejuvenation, in part, of the immune system and alleviation of many pathologies associated with HIV infection with or without progression to AIDS. However, serious metabolic complications and end-organ damage are now emerging as new threats to long-term survivors of HIV infection. Among the end-organ damage associated with ART is intensified skeletal deterioration [3–5, 14–18]. This occurs particularly within the first 2 years of ART initiation, when up to 6% of a patient's BMD may be lost

Received 9 May 2017; editorial decision 19 August 2017; accepted 23 August; 2017; published online August 25, 2017.

[a]M. N. W. and I. O. contributed equally as lead investigators.

[b]Present affiliation: Department of Pathology and Laboratory Medicine, David Geffen School of Medicine, University of California, Los Angeles.

Correspondence: M. Neale Weitzmann, PhD, Division of Endocrinology and Metabolism and Lipids, Department of Medicine, Emory University School of Medicine, 101 Woodruff Cir, 1305 WMRB, Decatur, GA 30322-0001 (mweitzm@emory.edu).

The Journal of Infectious Diseases® 2017;216:1070–9

DOI: 10.1093/infdis/jix444

over and above the bone already lost because of chronic HIV infection [15, 16].

Large population-based studies are now routinely reporting a significant overall 2–5-fold higher rate of fracture and HIV-infected patients, compared with age- and sex-matched uninfected patients [19–23]. Although all fractures can lead to significant morbidity, hip fractures are extremely serious and can be associated with mortality rates as high as 24%–33% within the first year of fracture [24–26]. Bone fractures thus have the potential to generate significant morbidity and mortality in HIV-infected patients receiving long-term ART, especially as the population continues to age.

Although aggressive bone loss has been attributed to drugs such as tenofovir disoproxil fumarate, emerging data suggest that a significant portion of ART-induced bone loss may be independent of specific ART regimen [27–30]. However, the molecular mechanisms involved remain unclear but may be mediated in large measure through indirect effects of ART on the immunoskeletal interface. We have reported that increased bone resorption in humans initiating ART is significantly associated with the degree of immune reconstitution achieved by individual subjects [14]. We have further modeled the process of immune regeneration associated with ART, using immunocompromised T-cell–deficient T-cell receptor β (TCRβ) knockout (KO) mice reconstituted with $CD3^+$ T cells [31]. These data suggested that inflammation in the bone microenvironment resulting from ART-mediated early T-cell repopulation and immune reconstitution may drive or exacerbate ART-associated bone loss.

In this study, we investigated the specific effects of $CD4^+$ and $CD8^+$ T-cell repopulation on bone turnover and loss of BMD and bone volume. Our data suggest that reconstituting the population of $CD4^+$ T cells, the dominantly affected population in HIV infection, elicits aggressive deterioration of both cortical and trabecular bone mass, while reconstituting subsets of $CD8^+$ T cells, a population that may also be diminished in patients with advanced AIDS, may also contribute to trabecular bone loss in some subjects.

METHODS

All animal studies were approved by the Emory University Institutional Animal Care and Use Committee and were conducted in accordance with the National Institutes of Health Laboratory Guide for the Care and Use of Laboratory Animals.

Mice were housed under specific-pathogen-free conditions and were fed γ-irradiated 5V02 mouse chow (Purina Mills) and autoclaved water ad libitum. The temperature of the animal facility was kept at 23°C (±1°C) with 50% relative humidity and a cycle of 12 hours of light followed by 12 hours of darkness.

T-Cell Adoptive Transfer

T cells were transplanted as previously described for $CD3^+$ T cells [31], with modifications. Briefly, $CD4^+$ or $CD8^+$ T cells were purified from the spleens of 6–8-week-old female C57BL6/J wild-type mice. $CD4^+$ T cells were purified by double purification using negative immunomagnetic isolation with CD4 negative immunomagnetic beads (Stemcell Technologies, Vancouver, BC, Canada), followed by depletion of $CD8^+$ T cells. For $CD8^+$ T-cell isolation, CD8 negative immunomagnetic purification was performed followed by removal of any contaminating $CD4^+$ T cells by positive immunomagnetic depletion, using CD4 immunomagnetic beads. All reagents and materials used in T-cell purification were endotoxin free and T cells were processed under sterile conditions. For adoptive transfer, purified $CD4^+$ or $CD8^+$ T cells (1×10^6 cells/mouse) were injected into the tail vein of syngeneic female C57BL6/J TCRβ KO mice aged 20 weeks. The tail vein of control (ie, sham) mice was injected with vehicle only (phosphate-buffered saline). Reconstitution of T-cell subsets and the degree of contamination of $CD4^+$ T cells with $CD8^+$ T cells or vice versa was assessed by flow cytometry at the time mice were euthanized (12 weeks after reconstitution; Supplementary Figure 1).

Bone Densitometry

BMD measurements were performed in anesthetized mice at baseline (0) and at 2, 4, 8, and 12 weeks following sham or T-cell reconstitution by dual-energy x-ray absorptiometry (DXA), using a PIXImus 2 bone densitometer (GE Medical Systems) as previously described [31]. Data (mean values ± standard errors of the mean [SEMs]) are presented as percentage changes in BMD for each individual mouse from baseline to each time point. For analysis of femurs and tibias, the left and right femurs or tibias were averaged for each individual mouse before calculating the mean femur or tibia BMD for all mice in the group.

Micro–Computed Tomography

Micro–computed tomography was performed in the L3 vertebral body and in the mid-diaphysis cortical bone) and distal metaphysis (trabecular bone) of the right femur ex vivo to assess cortical and trabecular bone volume and microarchitecture. Mice were euthanized, and bones were isolated by dissection, followed by soft-tissue removal. Bones were fixed and stored in 70% ethanol at 4°C until micro–computed tomography, using a microCT 40 scanner (Scanco Medical, Brüttisellen, Switzerland). The scanner was calibrated weekly with a factory-supplied phantom. A total of 405 tomographic slices at a voxel size of 6 μm (70 kVp and 114 mA, with 200 ms integration time) were taken at the L3 vertebra (total area, 2.43 mm). Trabecular bone was segmented from the cortical shell, beginning approximately 0.5 mm from the distal growth plate. Projection images were reconstructed using the auto-contour function for trabecular bone. Femoral cortical bone was quantified at the mid-diaphysis from 100 tomographic slices spanning 0.6 mm. Representative vertebral samples based on the mean ratio of the bone volume to the total volume were

reconstructed to generate 3-dimensional visual representations. Indices and units were standardized per published guidelines [32].

Biochemical Indices of Bone Turnover

Metabolic indices of bone resorption and bone formation were quantified in mouse serum obtained 12 weeks after T-cell transfer, using a RATlaps enzyme-linked immunosorbent assay (ELISA) for measurement of C-terminal telopeptide of type I collagen, a specific and sensitive marker of bone resorption, and a Rat-MID ELISA for measurement of osteocalcin, a specific and sensitive marker of bone formation (both from Immunodiagnostic Systems, Fountain Hills, AZ). Total RANKL, osteoprotegerin, and tumor necrosis factor α (TNF-α) levels were quantified in mice serum by using ELISAs from R&D Systems (Minneapolis, MN).

In Vitro Osteoclastogenesis Assays

Whole bone marrow was isolated from mice in the sham and reconstitution groups 12 weeks after adoptive transfer. Bone marrow cells from individual mice (n = 6) were plated into 96-well plates at a density of 1×10^5 nucleated cells/well, with 5 replicate wells for each individual mouse. Cells were cultured in 200 μL of alpha modified Eagle's medium supplemented with 10% fetal bovine serum and treated with M-CSF (25 ng/mL). Some wells received a low subsaturating dose (15 ng/mL) of RANKL (R & D Systems). Fifty percent of the medium was changed every 3 days, and fresh RANKL and/or M-CSF was added. After 9 days of culture, cells were fixed and stained for expression of tartrate resistant acid phosphatase. Multinucleated (≥3 nuclei) tartrate-resistant acid phosphatase–positive cells were defined as osteoclasts and quantitated under light microscopy, with normalization for size, based on the number of nuclei. Five replicate wells were quantified and averaged for each of 6 individual mice. Averages were used to calculate mean osteoclast number (±SEM) for each group.

Statistical Analysis

Statistical significance was determined using GraphPad Prizm 7.0 for Macintosh (GraphPad Software, La Jolla, CA). Simple comparisons were made using the Student *t* test. Multiple comparisons were performed by 1-way analysis of variance (ANOVA) with the Tukey multiple comparisons post hoc test. Prospective BMD data were analyzed by 2-way ANOVA with the Tukey multiple comparisons post hoc test to assess the significance of differences between the sham and $CD4^+$ T-cell–reconstituted groups and sham and $CD8^+$ T-cell–reconstituted groups at each time point. Gaussian distribution was assessed by the Shapiro-Wilk test. *P* values of ≤.05 were considered statistically significant.

In the osteocalcin assay, 2 values in the $CD8^+$ T cells group were below the level of detection. To allow for more-robust statistics, the nondetectable values were imputed using the L/2 substitution formula, where L is the limit of detection as described elsewhere [33]. The limit of detection for osteocalcin is 50 ng/mL, per the manufacturers data sheet (Immunodiagnostic Systems).

RESULTS

Reconstitution of $CD4^+$ but Not $CD8^+$ T Cells Induces Significant Loss of BMD, as Quantified by DXA

We have reported that $CD3^+$ T cells reconstituted at physiological ratios of $CD4^+$ and $CD8^+$ T cells elicit significant bone loss over 12 weeks during homeostatic repopulation into host TCRβ KO mice [31], modeling immune reconstitution bone loss sustained by HIV-infected patients initiating ART. To further study the independent effect of $CD4^+$ and $CD8^+$ T-cell reconstitution on bone turnover and mass, we independently reconstituted $CD4^+$ or $CD8^+$ T cells in TCRβ KO mice by syngeneic adoptive transfer with equivalent numbers (1×10^6) of each subset. Changes in BMD were quantified prospectively over 3 months, using in vivo DXA. Compared to sham-injected mice, mice receiving $CD4^+$ T cells underwent a robust and significant overall decline in total body BMD (Figure 1A) by 4 weeks after reconstitution. Independent analysis of lumber spine (Figure 1B), femurs (Figure 1C), and tibias (Figure 1D) also revealed significant bone loss beginning 4 or 8 weeks after $CD4^+$ T-cell reconstitution. By contrast, reconstitution with $CD8^+$ T cells failed to show a significant loss of BMD at any site (Figures 1A–1D).

Reconstitution of $CD4^+$ and $CD8^+$ T Cells Elicits Significant Trabecular Bone Loss, Whereas Only Reconstitution of $CD4^+$ T Cells Significantly Influences Cancellous Bone

Because DXA provides an integral measurement of cortical and trabecular bone mass and cortical bone represents approximately 80% of total BMD, the trabecular compartment is underestimated. To specifically quantify the cortical and cancellous bone compartments independently, we used high-resolution (6 μm) micro–computed tomography of femurs and vertebrae ex vivo 12 weeks after T-cell reconstitution.

Three-dimensional micro–computed tomographic reconstructions of femoral diaphysis (Figure 1A) revealed significant loss of cortical bone mass in mice in which the $CD4^+$ T-cell population was reconstituted but not in mice transplanted with $CD8^+$ T cells. By contrast, transplantation of $CD4^+$ or $CD8^+$ T cells both caused significant deterioration of trabecular bone mass (Figure 2A). An identical trend was observed in vertebrae (Figure 2B).

Visual representations of bone changes were confirmed by detailed microarchitectural quantification of trabecular and cortical bone parameters in the femur (Table 1) and vertebrae (Table 2) for $CD4^+$ and $CD8^+$ T-cell–reconstituted mice. The data confirm a significant decline in the trabecular bone volume fraction in both $CD4^+$ T-cell– and $CD8^+$ T-cell–reconstituted mice in both femur (Table 1) and vertebrae (Table 2).

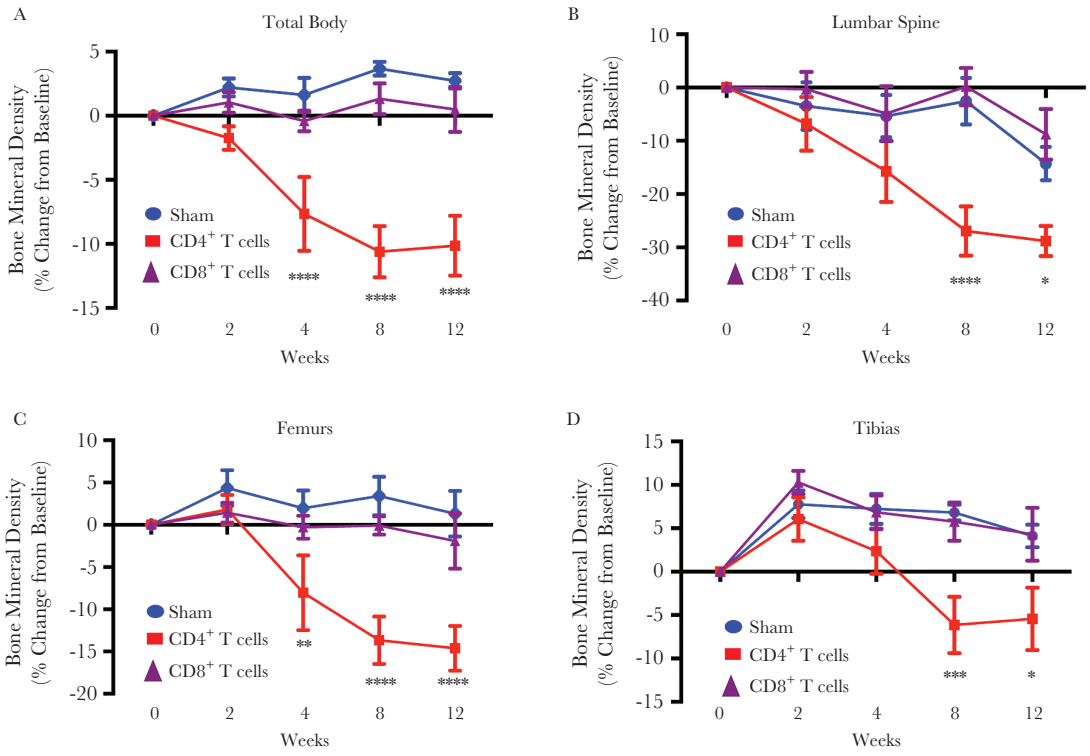

Figure 1. Prospective bone mineral density in mice transplanted with CD4⁺ or CD8⁺ T cells. Bone mineral density (BMD) total body (*A*) and in the lumbar spine (*B*), femur (average of left and right femur for each mouse; *C*), and tibia (average of left and right tibia for each mouse; *D*) was quantified by dual-energy x-ray absorptiometry at baseline (0 weeks) and 2, 4, 8 and 12 weeks following CD4⁺ T-cell or CD8⁺ T-cell adoptive transfer. All data are expressed as means ± standard errors of the mean. Data are for 12 mice in the sham group and 6 mice each in the CD4⁺ and CD8⁺ T-cell–reconstituted groups. **P* < .05, ***P* < .01, ****P* < .001, *****P* < .0001, compared with the sham group, by 2-way analysis of variance with the Tukey multiple comparisons post hoc test.

In the femur, the trabecular structural index and trabecular number were significantly decreased in both CD4⁺ and CD8⁺ T-cell groups in the femur, leading to an expected increase in trabecular separation. Trabecular thickness was diminished in both groups but not significantly. Interestingly, the reverse was observed in the vertebrae, with trabecular number being more robustly affected than trabecular thickness.

CD4⁺ T-cell–reconstituted mice also displayed a significant decline in cortical indices, including cortical bone area, average cortical thickness, total cross-sectional area inside the periosteal envelope, and cortical area fraction. Mice in which the CD8⁺ T-cell population was reconstituted showed only relatively small declines in cortical structure that were not statistically significant for any index in the femur (Table 1). Data were similar for the vertebrae (Table 2), although declines in cortical thickness in recipients of CD8⁺ T-cell transplants reached statistical significance, but the magnitude of decline was approximately 50% of that observed in the CD4⁺ T-cell transplant recipients.

Our data support the DXA outcomes and reveal that CD4⁺ T cells promote both trabecular and cortical bone loss, while the dominant effect of CD8⁺ T cells was on trabecular bone, with only relatively modest and mostly nonsignificant changes in cortical bone.

CD4⁺ but Not CD8⁺ T-Cell Reconstitution Enhances Biochemical Indices of Bone Resorption In Vivo

The index of bone resorption serum C-terminal telopeptide of type I collagen was quantified in mice 12 weeks after adoptive transfer and was significantly elevated in CD4⁺ but not CD8⁺ T-cell–reconstituted mice (Figure 3A). As circulating markers reflect turnover across the entire skeleton, which is predominantly cortical bone, the data are consistent with the lack of cortical bone loss observed by DXA and micro–computed tomography in CD8⁺ T cells.

No significant change in serum osteocalcin, a marker of bone formation, was observed for either reconstituted CD4⁺ or CD8⁺ T cells (Figure 3B).

RANKL, but Not Osteoprotegerin, Is Significantly Elevated in the Serum of CD4⁺ and CD8⁺ T-Cell–Reconstituted Mice

Because RANKL is the key osteoclastogenic cytokine and its activity is moderated by its decoy receptor osteoprotegerin, we quantified circulating RANKL and osteoprotegerin levels in the serum of sham-exposed mice and CD4⁺ and CD8⁺ T-cell–reconstituted mice. Serum RANKL level was significantly elevated in both CD4⁺ and CD8⁺ T-cell–reconstituted mice (Figure 3C), while the osteoprotegerin level (Figure 3D)

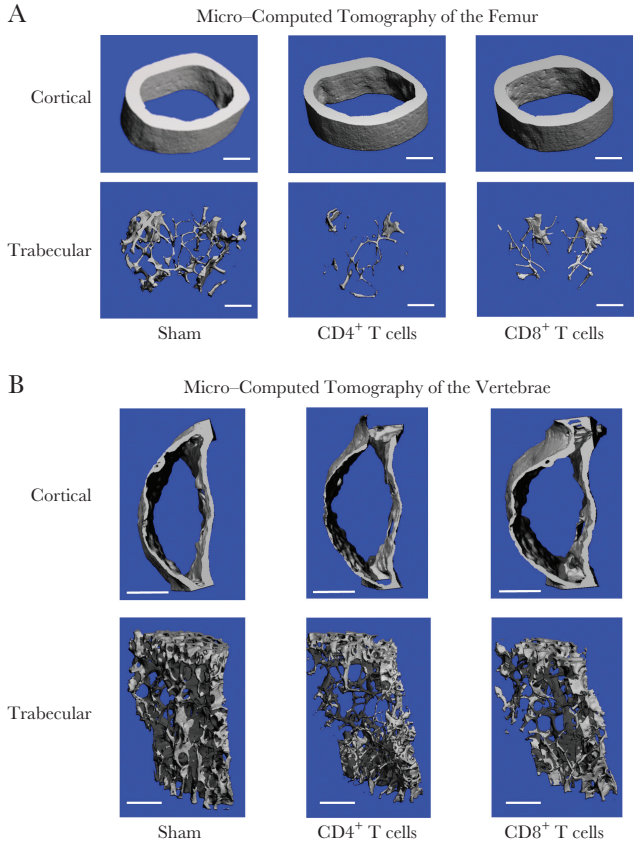

Figure 2. Representative cortical and trabecular bone reconstructions from CD4+ or CD8+ T-cell–reconstituted mice by micro–computed tomography. Representative cortical (upper panels) and trabecular (lower panels) high-resolution (6-μm) 3-dimensional reconstructions of femurs (*A*) and vertebrae (*B*) from mice in the sham group and those in CD4+ and CD8+ T-cell–reconstituted groups 12 weeks after reconstitution. The length of the white scale bar represents 500 μm.

was not significantly changed in either group as compared to the sham group.

Ex Vivo Osteoclast Formation Is Significantly Elevated in CD4+ but Not CD8+ T-Cell–Reconstituted Mice

To assess the osteoclastogenic potential of CD4+ and CD8+ T-cell–reconstituted bone marrow, we isolated whole bone marrow from all groups of mice 12 weeks after adoptive transfer and performed ex vivo osteoclastogenesis studies. In the absence of exogenous RANKL, bone marrow derived from CD4+ T-cell–transplant recipients generated significantly higher numbers of osteoclasts, compared with findings for the sham group, while CD8+ T-cell–reconstituted bone marrow was not significantly different to that in the sham group (Figure 4A). Addition of a low sub-saturating dose of RANKL raised the baseline of osteoclast formation in both Sham and CD8+ T-cell transplanted groups, however no significant differences were evident. Osteoclast formation by CD4+ T-cell transplanted bone marrow was only marginally increased by exogenous RANKL stimulation, suggesting that near saturating concentrations of RANKL were already being generated endogenously due to the presence of CD4+ T cells (Figure 4B).

Taken together our data reveal complex effects of independent CD4+ and CD8+ T-cell reconstitution with CD8+ T cells impacting predominantly trabecular bone while CD4+ T cells robustly affect both cortical and cancellous compartments (Figure 2 and Tables 1 and 2).

DISCUSSION

We recently reported that adoptive transfer of CD3+ T cells containing physiological ratios of both CD4+ and CD8+ T cells into TCRβ KO mice led to dramatic loss of BMD and bone volume [31]. We suggested that the processes of homeostatic T-cell repopulation and immune reconstitution mimic that of ART-induced T-cell recovery in HIV-infected humans and provide a plausible mechanism to explain in part the bone loss common to all ART regimens [31]. Although in humans, T-cell recovery is predominantly CD4+ T cells, in very advanced cases of HIV infection CD8+ T cells may also be diminished.

We previously, adoptively transferred CD3+ T cells, containing a population of CD4+ and CD8+ T-cell subsets. In this study, we further investigated the relative potential of CD4+ and CD8+ T-cell subsets to influence bone loss after T-cell reconstitution. Our data reveal that although both subsets have the capacity to contribute significantly to bone loss, CD8+ T cells mediate effects that were mostly limited to the trabecular compartment. By contrast, CD4+ T cells induce robust loss of both cortical and trabecular bone. One possible explanation for this differential effect lies in the relative production of RANKL and TNF by CD4+ and CD8+ T cells in the bone marrow microenvironment.

Another reason that CD4+ T cells may be more osteoclastogenic than CD8+ T cells is that CD4+ T cells are the lynchpin of adaptive immunity, and their restoration is likely to rejuvenate humoral immunity through B-cell reactivation, as well as rekindling general antigen presentation to professional antigen-presenting cells (ie, macrophages, dendritic cells, and B cells). Indeed, we have reported that in response to T-cell reconstitution in immunodeficient mice, B cells and macrophages produce significant concentrations of TNF that likely contribute to bone resorption [31].

DXA is the gold standard for quantifying BMD across large bone surfaces and is used clinically for assessment of bone condition and clinical diagnosis of osteopenia and osteoporosis. BMD quantified by DXA revealed significant bone loss following CD4+ T-cell transplantation but not with CD8+ T-cell adoptive transfer. High-resolution micro–computed tomography, however, identified significant deterioration of the trabecular bone compartment in both CD4+ and CD8+ T-cell–reconstituted mice, but only cortical bone was significantly impacted by CD4+ T-cell transplants.

Table 1. Femoral Structural Indices Determined by Micro–Computed Tomography in Control (Sham) and CD4+ and CD8+ T-Cell–Reconstituted Mice

Index	CD4+ T-Cell–Associated Comparison, Mean ± SD				CD8+ T-Cell–Associated Comparison, Mean ± SD			
	Sham Group	Reconstituted Group	Percentage Change	Exact *P*[a]	Sham Group	Reconstituted Group	Percentage Change	Exact *P*[a]
Trabecular								
Total volume, mm^3	1.27 ± 0.07	1.41 ± 0.06	+11.1	≤.0025	1.26 ± 0.06	1.36 ± 0.09	+7.2	≤.0682
Bone volume, mm^3	0.060 ± 0.011	0.026 ± 0.006	−56.7	≤.0001	0.062 ± 0.012	0.028 ± 0.007	−52.7	≤.0001
Bone volume fraction, %	4.75 ± 0.01	1.85 ± 0.41	−61.2	≤.0001	4.88 ± 0.01	2.07 ± 0.42	−54.6	≤.0001
Trabecular thickness, mm	0.041 ± 0.003	0.036 ± 0.005	−11.8	≤.0793	0.041 ± 0.003	0.036 ± 0.005	−12.4	≤.0507
Trabecular number, /mm[b]	3.20 ± 0.20	2.49 ± 0.12	−22.1	≤.0001	3.22 ± 0.19	2.67 ± 0.12	−16.4	≤.0003
Trabecular separation, mm	0.316 ± 0.022	0.407 ± 0.018	+31.8	≤.0001	0.313 ± 0.021	0.382 ± 0.014	+20.9	≤.0001
Cortical								
Cortical area, mm^2	0.879 ± 0.049	0.748 ± 0.041	−15.0	≤.0006	0.879 ± 0.049	0.829 ± 0.094	−5.7	≤.2802
Cortical thickness, mm	0.192 ± 0.012	0.159 ± 0.009	−17.5	≤.0003	0.192 ± 0.012	0.180 ± 0.014	−6.4	≤.1320
Total cross-sectional area, mm^3	0.497 ± 0.028	0.421 ± 0.024	−15.4	≤.0006	0.497 ± 0.028	0.459 ± 0.036	−7.8	≤.0683
Cortical area fraction, %	176.8 ± 0.4	177.8 ± 0.5	+0.6	≤.0022	176.8 ± 0.4	180.4 ± 8.1	+2.0	≤.3284

Data for 6 mice per group.

[a]By the Student *t* test.

[b]Calculated as the inverse of the mean distance between the mid-axes of the femur.

These data highlight a significant caveat of DXA technology. DXA provides an integrated measurement of both cortical and trabecular compartments, but the adult human skeleton is composed of 80% cortical bone and only 20% trabecular bone, although different skeletal sites have different ratios of cortical to trabecular bone [34]. For example, vertebra are trabecular-rich sites with a cortical bone to trabecular bone ratio of 25:75, while the ratio in the femoral head is 50:50 and that in the radial diaphysis is 95:5 [34]. Consequently, DXA is not a sensitive technology for quantifying changes in trabecular

Table 2. Vertebral Structural Indices Determined by Micro–Computed Tomography in Control (Sham) and CD4+ and CD8+ T-Cell–Reconstituted Mice

Index	CD4+ T-Cell–Associated Comparison, Mean ± SD				CD8+ T-Cell–Associated Comparison, Mean ± SD			
	Sham Group	Reconstituted Group	Percentage Change	Exact *P*[a]	Sham Group	Reconstituted Group	Percentage Change	Exact *P*[a]
Trabecular								
Total volume, mm^3	3.23 ± 0.26	3.68 ± 0.41	+14.1	≤.0434	3.23 ± 0.26	3.45 ± 0.11	+7.0	≤.0805
Bone volume, mm^3	0.477 ± 0.139	0.389 ± 0.041	−18.4	≤.1670	0.477 ± 0.139	0.433 ± 0.051	−9.2	≤.4816
Bone volume fraction, %	14.6 ± 2.9	10.6 ± 0.61	−27.5	≤.0071	14.6 ± 2.9	12.6 ± 1.6	−13.9	≤.1589
Trabecular thickness, mm	0.041 ± 0.002	0.033 ± 0.002	−18.6	≤.0001	0.041 ± 0.002	0.037 ± 0.004	−9.5	≤.0546
Trabecular number, /mm[b]	4.13 ± 0.70	3.51 ± 0.17	−15.1	≤.0600	4.13 ± 0.70	3.93 ± 0.32	−4.9	≤.5306
Trabecular separation, mm	0.248 ± 0.032	0.291 ± 0.016	+17.3	≤.0141	0.248 ± 0.032	0.261 ± 0.023	+5.3	≤.4287
Cortical								
Cortical area, mm^2	0.323 ± 0.022	0.254 ± 0.022	−21.4	≤.0003	0.323 ± 0.022	0.305 ± 0.060	−5.5	≤.5140
Cortical thickness, mm	0.063 ± 0.003	0.048 ± 0.005	−22.9	≤.0001	0.063 ± 0.003	0.055 ± 0.007	−12.0	≤.0406
Total cross-sectional area, mm^3	0.779 ± 0.080	0.602 ± 0.066	−22.8	≤.0018	0.779 ± 0.080	0.703 ± 0.140	−9.7	≤.2771
Cortical area fraction, %	41.6 ± 1.5	42.3 ± 1.0	1.6	≤.3753	41.6 ± 1.5	43.4 ± 0.5	+4.5	≤.0163

Data for 6 mice per group.

[a]By the Student *t* test.

[b]Calculated as the inverse of the mean distance between the mid-axes of the vertebrae.

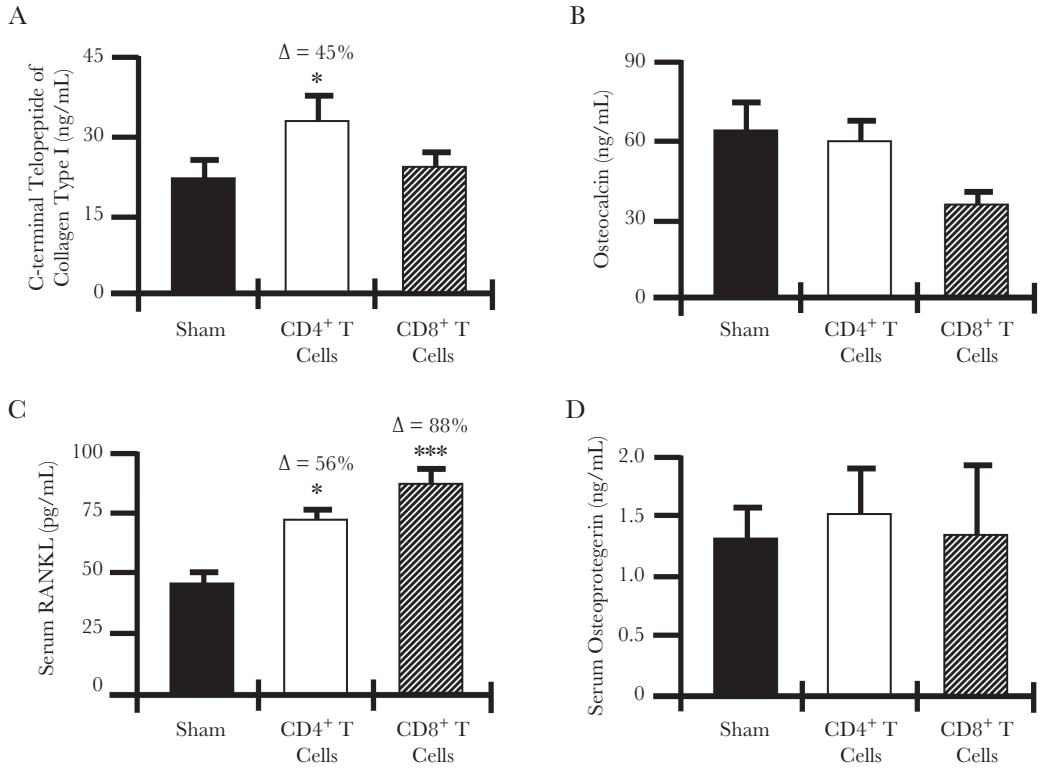

Figure 3. Biochemical bone turnover markers and circulating osteoclastogenic cytokines. Serum from sham-exposed mice and CD4+ and CD8+ T-cell–reconstituted mice was collected 12 weeks after reconstitution for quantification of biochemical markers of bone resorption (ie, C-terminal telopeptide of type I collagen; *A*) and bone formation (ie, osteocalcin; *B*). Serum cytokines representing the key final osteoclastogenic effectors were quantified by enzyme-linked immunosorbent assay for receptor activator of nuclear factor κB ligand (RANKL; *C*) and osteoprotegerin (*D*). Data are expressed as means ± standard errors of the mean. Data are for 6 mice/group. Δ, percentage change from the sham group. **P* < .05 and ****P* < .001, compared with the sham group, by 1-way analysis of variance with the Tukey multiple comparisons post hoc test.

bone. As the trabecular bone compartment is considerably more metabolically active than cortical bone and also contributes to load-bearing capacity, DXA-based measurements may significantly underestimate the extent of skeletal deterioration. Indeed, it has been reported that about half of hip fractures occur in women who are not osteoporotic based on BMD testing by DXA [35]. The inability of DXA to assess trabecular condition or to estimate bone quality aspects may contribute to its poor sensitivity.

C-terminal telopeptide of type I collagen is a sensitive and specific biochemical index of global bone resorption in the body, but it quantifies bone resorption averaged across all bone

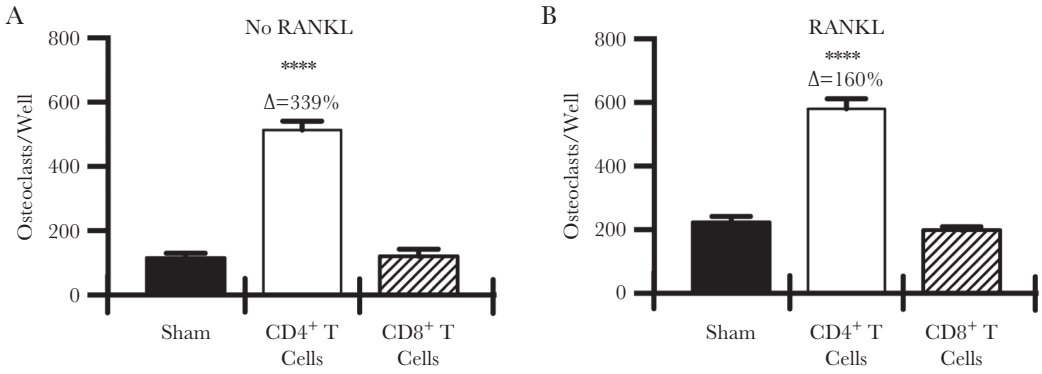

Figure 4. Ex vivo osteoclastogenesis assays. Ex vivo osteoclastogenesis assays were performed in the absence of exogenous receptor activator of nuclear factor κB ligand (RANKL; *A*) or in the presence of a low subsaturating dose of RANKL (15 ng/mL; *B*). Osteoclasts were differentiated from whole bone marrow from individual mice (6 mice/group) with 5 replicates per mouse. All wells received macrophage colony-stimulating factor (25 ng/mL). *****P* < .0001 compared with the sham group, by 1-way analysis of variance with the Tukey multiple comparisons post hoc test. Δ, percentage change from the sham group.

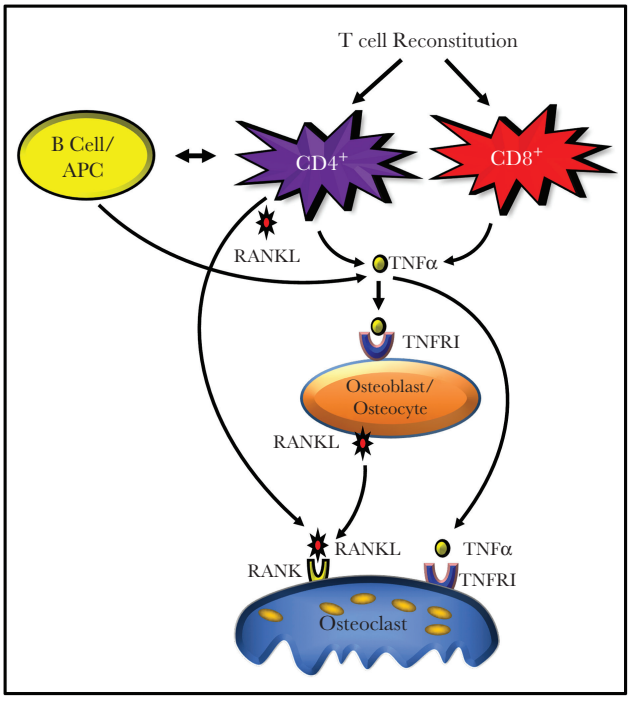

Figure 5. Model of CD4+ and CD8+ T-cell effects on osteoclastic bone resorption. Homeostatic reconstitution of CD4+ T cells leads to production of both tumor necrosis factor (TNF) and receptor activator of nuclear factor κB ligand (RANKL) in the bone marrow microenvironment. TNF amplified RANKL activity and promoted additional RANKL production by osteoblast-lineage cells, driving cortical and trabecular bone loss. CD8+ T cells produce only TNF in the bone marrow, inducing relatively modest levels of RANKL from osteoblasts and driving trabecular bone loss only. In addition, reconstitution of CD4+ T cells further leads to reinitiating of adaptive immune responses, including humoral immunity and antigen-presentation activity, that lead to additional TNF production by B cells and other antigen-presenting cells (APCs), such as macrophages. This potent inflammatory activity of CD4+ T cells likely drives a critical threshold of RANKL and TNF that is capable of driving cortical bone resorption. TNFR1, TNF receptor 1.

surfaces. Consistent with this concept, the level of C-terminal telopeptide of type I collagen was observed to be elevated in CD4+ T-cell–reconstituted mice but was not altered in CD8+ T-cell–reconstituted mice, despite significant trabecular bone loss. Like DXA measurements, biochemical bone resorption markers significantly underestimate degradation of the trabecular compartment and this is the likely explanation for why quantifiable changes in resorption marker were not observed in the circulation in the CD8+ T-cell–reconstituted mice in which only trabecular bone was affected.

While these animal studies provide mechanistic insight into the osteoclastogenic activities of reconstituting CD4+ and CD8+ T cells, there are some important limitations in the model and in its interpretation. First, although the model provides proof of concept for immune reconstitution bone loss, it is an ART-free model. In humans, T-cell repopulation is a consequence of ART, and this model does not directly replicate this process. As HIV-transgenic animal models (rats and mice) are constitutively active, they are insensitive to ART. Future studies using a humanized mouse infected by HIV may be a more suitable model, although a caveat is that multiple steps involved in generation of humanized mice are themselves associated with bone loss, complicating interpretation.

Another limitation is T-cell reconstitution of a completely T-cell–deficient animal. Although this creates an aggressive homeostatic reconstitution event that leads to pronounced bone loss and is propitious for detailed mechanistic investigations in a mouse, it is likely an exaggeration of the more modest events associated with human immune reconstitution following ART. As previously reported by us, there is high variability in responses to ART in human subjects in terms of osteoclastogenic and inflammatory cytokine production and kinetics of changes [14], which are more homogenous in the mouse model. Nonetheless, the model allows for predictions to be made that can be tested in human populations. For example, patients with low nadir CD4+ and CD8+ T-cell counts are likely to sustain more-aggressive trabecular bone loss. Computed tomography or high-resolution computed tomography studies in progress may be able to validate these outcomes.

We recently completed a phase 2b trial in which all subjects initiating ART were treated with a single dose of the antiresorptive agent zoledronic acid (or placebo) [15]. Although this strategy was extremely effective in blocking bone loss, being able to predict the degree of bone loss likely to be unleashed by ART, based on baseline T-cell populations and/or their early cytokine production profiles and/or ratios of CD4+ T cells to CD8+ T cells, may allow for a more tailored and personalized approach to treatment.

In conclusion, our cumulative data demonstrate that repopulation of CD4+ T cells leads to significant increases in levels of both RANKL and TNF that promote robust bone resorption, affecting both trabecular and cortical compartments. By contrast, reconstituting CD8+ T cells increase bone marrow TNF levels only, supporting predominantly trabecular bone loss. In humans undergoing ART, repopulation of the depleted CD4+ T-cell population may contribute significantly to bone resorption and both cortical and trabecular bone loss. In subjects with advanced AIDS and CD8+ T-cell depletion, reconstituting CD8+ T cells may further contribute to trabecular bone loss.

Supplementary Data

Supplementary materials are available at *The Journal of Infectious Diseases* online. Consisting of data provided by the authors to benefit the reader, the posted materials are not copyedited and are the sole responsibility of the authors, so questions or comments should be addressed to the corresponding author.

Notes

Acknowledgment. We thank Dr Daiana Weiss (Emory University) for critical reading of the manuscript.

Disclaimer. The content is solely the responsibility of the authors and does not represent the official views of the National Institutes of Health or the Department of Veterans Affairs.

Financial support. This work was supported by the National Institute of Arthritis and Musculoskeletal and Skin Diseases (grants R01AR059364, R01AR068157, and R01AR070091), the National Institute on Aging (award R01AG040013 to M. N. W. and I. O.), and the National Institute of Allergy and Infectious Diseases (grant K23A1073119 to I. O.), National Institutes of Health; and by the Biomedical Laboratory Research and Development Service, Department of Veterans Affairs Office of Research and Development (grant 5I01BX000105 to M. N. W.).

Potential conflicts of interest. All authors: No reported conflicts of interest. All authors have submitted the ICMJE Form for Disclosure of Potential Conflicts of Interest. Conflicts that the editors consider relevant to the content of the manuscript have been disclosed.

References

1. Khosla S. Minireview: the OPG/RANKL/RANK system. Endocrinology **2001**; 142:5050–5.
2. Teitelbaum SL. Bone resorption by osteoclasts. Science **2000**; 289:1504–8.
3. Tebas P, Powderly WG, Claxton S, et al. Accelerated bone mineral loss in HIV-infected patients receiving potent antiretroviral therapy. AIDS **2000**; 14:F63–7.
4. Thomas J, Doherty SM. HIV infection–a risk factor for osteoporosis. J Acquir Immune Defic Syndr **2003**; 33:281–91.
5. Ofotokun I, Weitzmann MN. HIV-1 infection and antiretroviral therapies: risk factors for osteoporosis and bone fracture. Curr Opin Endocrinol Diabetes Obes **2010**; 17:523–9.
6. Stone B, Dockrell D, Bowman C, McCloskey E. HIV and bone disease. Arch Biochem Biophys **2010**; 503:66–77.
7. Arora S, Agrawal M, Sun L, Duffoo F, Zaidi M, Iqbal J. HIV and bone loss. Curr Osteoporos Rep **2010**; 8:219–26.
8. Ofotokun I, Weitzmann MN. HIV and bone metabolism. Discov Med **2011**; 11:385–93.
9. Brown TT, Qaqish RB. Antiretroviral therapy and the prevalence of osteopenia and osteoporosis: a meta-analytic review. AIDS **2006**; 20:2165–74.
10. Bonjoch A, Figueras M, Estany C, et al.; Osteoporosis Study Group. High prevalence of and progression to low bone mineral density in HIV-infected patients: a longitudinal cohort study. AIDS **2010**; 24:2827–33.
11. Sharma A, Flom PL, Weedon J, Klein RS. Prospective study of bone mineral density changes in aging men with or at risk for HIV infection. AIDS **2010**; 24:2337–45.
12. Vikulina T, Fan X, Yamaguchi M, et al. Alterations in the immuno-skeletal interface drive bone destruction in HIV-1 transgenic rats. Proc Natl Acad Sci U S A **2010**; 107:13848–53.
13. Titanji K, Vunnava A, Sheth AN, et al. Dysregulated B cell expression of RANKL and OPG correlates with loss of bone mineral density in HIV infection. PLoS Pathog **2014**; 10:e1004497.
14. Ofotokun I, Titanji K, Vunnava A, et al. Antiretroviral therapy induces a rapid increase in bone resorption that is positively associated with the magnitude of immune reconstitution in HIV infection. AIDS **2016**; 30:405–14.
15. Ofotokun I, Titanji K, Lahiri CD, et al. A single-dose zoledronic acid infusion prevents antiretroviral therapy-induced bone loss in treatment-naive HIV-infected patients: a phase IIb trial. Clin Infect Dis **2016**; 63:663–71.
16. McComsey GA, Tebas P, Shane E, et al. Bone disease in HIV infection: a practical review and recommendations for HIV care providers. Clin Infect Dis **2010**; 51:937–46.
17. Yin MT, McMahon DJ, Ferris DC, et al. Low bone mass and high bone turnover in postmenopausal human immunodeficiency virus-infected women. J Clin Endocrinol Metab **2010**; 95:620–9.
18. Bolland MJ, Grey A. HIV and low bone density: responsible party, or guilty by association? IBMS BoneKEy **2011**; 8:7–15.
19. Triant VA, Brown TT, Lee H, Grinspoon SK. Fracture prevalence among human immunodeficiency virus (HIV)-infected versus non-HIV-infected patients in a large U.S. healthcare system. J Clin Endocrinol Metab **2008**; 93:3499–504.
20. Prior J, Burdge D, Maan E, et al. Fragility fractures and bone mineral density in HIV positive women: a case-control population-based study. Osteoporos Int **2007**; 18:1345–53.
21. Young B, Dao CN, Buchacz K, Baker R, Brooks JT. Increased rates of bone fracture among HIV-infected persons in the HIV outpatient study (HOPS) compared with the US general population, 2000–2006. Clin Infect Dis **2011**; 52:1061–8.
22. Womack JA, Goulet JL, Gibert C, et al.; Veterans Aging Cohort Study Project Team. Increased risk of fragility fractures among HIV infected compared to uninfected male veterans. PLoS One **2011**; 6:e17217.
23. Prieto-Alhambra D, Güerri-Fernández R, De Vries F, et al. HIV infection and its association with an excess risk of clinical fractures: a nationwide case-control study. J Acquir Immune Defic Syndr **2014**; 66:90–5.
24. Lewis JR, Hassan SK, Wenn RT, Moran CG. Mortality and serum urea and electrolytes on admission for hip fracture patients. Injury **2006**; 37:698–704.
25. Todd CJ, Freeman CJ, Camilleri-Ferrante C, et al. Differences in mortality after fracture of hip: the east Anglian audit. BMJ **1995**; 310:904–8.

26. Bass E, French DD, Bradham DD, Rubenstein LZ. Risk-adjusted mortality rates of elderly veterans with hip fractures. Ann Epidemiol **2007**; 17:514–9.
27. Brown TT, McComsey GA, King MS, Qaqish RB, Bernstein BM, da Silva BA. Loss of bone mineral density after antiretroviral therapy initiation, independent of antiretroviral regimen. J Acquir Immune Defic Syndr **2009**; 51:554–61.
28. Piso RJ, Rothen M, Rothen JP, Stahl M. Markers of bone turnover are elevated in patients with antiretroviral treatment independent of the substance used. J Acquir Immune Defic Syndr **2011**; 56:320–4.
29. Tebas P, Umbleja T, Dube MP, et al. Initiation of ART is associated with bone loss independent of the specific ART regimen: Results of ACTG A5005s. 14th Conference on Retroviruses and Opportunistic Infections **2007**:837.
30. Bruera D, Luna N, David DO, Bergoglio LM, Zamudio J. Decreased bone mineral density in HIV-infected patients is independent of antiretroviral therapy. AIDS **2003**; 17:1917–23.
31. Ofotokun I, Titanji K, Vikulina T, et al. Role of T-cell reconstitution in HIV-1 antiretroviral therapy-induced bone loss. Nat Commun **2015**; 6:8282.
32. Bouxsein ML, Boyd SK, Christiansen BA, Guldberg RE, Jepsen KJ, Müller R. Guidelines for assessment of bone microstructure in rodents using micro-computed tomography. J Bone Miner Res **2010**; 25:1468–86.
33. Hornung RW, Reed LD. Estimation of average concentration in the presence of nondetectable values. Appl Occup Environ Hyg **1990**; 5:46–51.
34. Clarke B. Normal bone anatomy and physiology. Clin J Am Soc Nephrol **2008**; 3(Suppl 3):S131–9.
35. Geusens P, van Geel T, van den Bergh J. Can hip fracture prediction in women be estimated beyond bone mineral density measurement alone? Ther Adv Musculoskelet Dis **2010**; 2:63–77.